ENGN 2290: A Micromechanical Model for Finite Rubber Viscoelasticity

Pinkesh Malhotra, Alexander Landauer

May 13, 2016

1 Introduction

1.1 Background

Soft rubbery materials are regularly used in engineering applications; thus, understanding and accurate modeling of the constitutive response of elastic and viscoelastic materials is an important topic of research. Purely elastic response characteristics are the result of static polymer networks, in which no relatively motion of polymer chain crosslinking occurs during deformation, whereas viscoelasticity arises due to transient polymer networks, in which crosslink bonds and entanglements can be permanently altered under physical deformations. Numerous models for both static and transient network polymers exist.

1.2 Proposed Work

Here we numerically implement a transient network model described in Linder et al. 2011 [1]. The ABAQUS (Dassault Systemes, Waltham, MA) UMAT interface is used to construct a finite element solution framework.

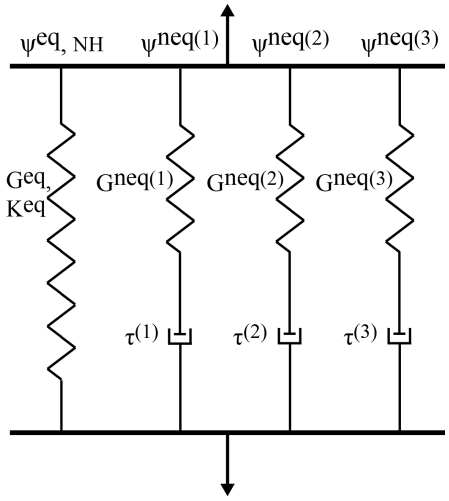

Figure 1: *The rheological analog diagram for our model. Three transient branches (denoted* neq*) are paired with a neo-hookean equilibrium spring (denoted* eq*). Eight parameters, as shown, are needed to fully specify the response.*

The UMAT requires that stresses, internal variables, and algorithmically consistent tangent moduli be updated in each step, and provides the prior values of these variable as input, in addition to the current deformation gradient. In this implementation, a neo-hookean equilibrium branch and three transient branches modeled after Linder et al. is utilized, in the form of the Maxwell-type rheological model shown in figure 1. Eight material properties (two equilibrium, six non-equilibrium) are needed.

1.3 Model Micromechanics

The equilibrium thermodynamics of the Linder et al. non-equilibrium branch rely on the freely jointed chain model, as described by Doi and Edwards [2]. The probability distribution function (PDF) that describes the end-to-end vector of the polymer chain, given in terms of the magnitude (r) and mean square value (r_0^2) of the vector, is in the form of a Gaussian. By understanding this distribution as a quantification of the number of configurations allowed to the chain, the entropy of the system can be found. Thus, the polymer chain is an entropic spring, and the force required to stretch the molecule is given by

$$F_r = 3k_B\theta\frac{r}{r_0^2} \tag{1}$$

where k_B is the Boltzmann constant and θ is the temperature. This simple model precludes viscus effects.

To incorporate viscus effects, a polymer chain is introduced in which the endpoints are considered to be Brownian particles embedded in a viscus medium. The chain endpoints follow a Smoluchowski diffusion-type equation that is inherently dissipative. This formulation is applied to the polymer system by considering each point-like particle of the Smoluchowski model to instead be a chain, parameterized by several state variables rather than position only. Hence, the viscus stretch rate of the polymer follows

$$\langle \dot{\boldsymbol{\lambda}} \rangle = \dot{\mathbf{F}}\mathbf{F}^{-1}\boldsymbol{\lambda} - \frac{2k_B\theta}{\eta r_0^2}\nabla_\lambda \left(\ln p(\boldsymbol{\lambda}, t) + \frac{3}{2}\boldsymbol{\lambda}^2 \right) \tag{2}$$

where $\boldsymbol{\lambda} = \frac{\mathbf{r}}{r_0^2}$, $\mathbf{F}$ is the macroscopic deformation gradient, η is the viscosity, and $p(\boldsymbol{\lambda}, t)$ is the PDF that describes the state of the large number of chains near a material point.

The stretch rate is then used as continuum expression by creating a mapping ($\mathbf{P}$) between the undeformed and deformed microscale stretch spaces (parameterized by $\boldsymbol{\lambda}$) of the polymer model, which is clearly related to the macroscale deformation ($\mathbf{F}$) and viscus effects (η). The information in this mapping is fully captured via $\mathbf{A} = \mathbf{P}\mathbf{P}^T$, and thus the evolution of the viscus subnetwork follows

$$\dot{\mathbf{A}} = \frac{1}{\tau}\left(\bar{\mathbf{F}}^T\bar{\mathbf{F}}^{-1} - \mathbf{A} \right) \tag{3}$$

where the characteristic time-scale of the subnetwork (τ) is given by $\frac{1}{\tau} = \frac{12k_B\theta}{\eta r_0^2}$. Homogenization of the free energy, found by integrating the chemical potential derived from Eq. 2 over $\mathbb{R}^3$, in the stretch space gives a macroscopic free energy which is simplified to give

$$\psi^{neq} = \frac{G^{neq}}{2}\left[(\mathbf{A} : \bar{\mathbf{C}} - 3) - \ln|\det(\mathbf{A})| \right] \tag{4}$$

where $G^{neq} = nk_B\theta$ is the non-equilibrium modulus (n is the number of neighborhood chains).

2 Continuum Stresses and Tangents

2.1 Mechanical Free Energy

The mechanical free energy in the polymer network can be split into equilibrium and non-equilibrium free energies. The equilibrium free energy is due to the response of the ground network, while the transient network contributes to the non-equilibrium free energy only. Thus, the energy is decomposed as

$$\psi = \psi^{eq} + \psi^{neq} \tag{5}$$

$$\psi^{eq}_{NH} = \frac{G^{eq}}{2}(\bar{I}_1 - 3) + \frac{K}{2}(J-1)^2 \tag{6}$$

$$\psi^{neq} = \sum_{\alpha=1}^{N} \frac{G^{neq}}{2}\left[(\mathbf{A}^\alpha : \bar{\mathbf{C}} - 3) - \ln(\det(\mathbf{A}^\alpha)) \right] \tag{7}$$

where N is the number of non-equilibrium branches, G^{eq} is the neo-hookean equilibrium shear modulus, G^{neq} is the non-equilibrium shear modulus, K is the bulk modulus, $J = \det\mathbf{F}$, $\mathbf{A}^\alpha$ is the intermediate symmetric tensor discussed in §1.3 for the subnetwork α, and $\bar{\mathbf{C}} = \bar{\mathbf{F}}^T\bar{\mathbf{F}}$ is the isochoric right Cauchy Green tensor. The non-equilibrium free energy contributes only to the distortional portion of the total free energy.

2.2 Cauchy Stress

Cauchy stress can be found from mechanical free energy as

$$\mathbf{T} = 2J^{-1}\mathbf{F}\frac{\partial\psi(\mathbf{C},\mathbf{A}^{(\alpha)})}{\partial\mathbf{C}}\mathbf{F}^T = J^{-1}\frac{\partial\hat{\psi}(\mathbf{F})}{\partial\mathbf{F}}\mathbf{F}^T. \tag{8}$$

Since the equilibrium and non-equilibrium free energies are additive, the Cauchy stress for the two can be separately calculated and added

$$\mathbf{T}^{eq}_{NH} = \frac{G^{eq}}{2J}\big[\bar{\mathbf{B}} - \frac{tr(\bar{\mathbf{B}})}{3}\mathbf{I}\big] + [K(J-1)J]\mathbf{I} \tag{9}$$

$$\mathbf{T}^{neq(\alpha)} = J^{-1}G^{neq(\alpha)}\big[\bar{\mathbf{F}}\mathbf{A}^{(\alpha)}\bar{\mathbf{F}}^T - \frac{1}{3}(\mathbf{A}^{(\alpha)}:\bar{\mathbf{C}})\mathbf{I}\big] = J^{-1}G^{neq(\alpha)}\left[\mathbf{Q} - \frac{1}{3}R\mathbf{I}\right] \tag{10}$$

where $\bar{\mathbf{B}}$ is distortional part of the left Cauchy Green tensor, $\mathbf{Q} = \bar{\mathbf{F}}\mathbf{A}^{(\alpha)}\bar{\mathbf{F}}^T$, and $\mathbf{R} = \mathbf{A}^{(\alpha)}:\bar{\mathbf{C}}$.

2.3 Tangents

The algorithmically consistent tangent modulus required by ABAQUS is computed via

$$\mathbb{C}_{ijkl} = \frac{J^{-1}}{2}(F_{lm}\frac{dT_{K,ij}}{dF_{km}} + F_{km}\frac{dT_{K,ij}}{dF_{lm}}). \tag{11}$$

2.3.1 Tangent for Neo-Hookean Model

By applying the above definition to the Neo-Hookean constitutive model, the appropriate tangent is

$$\mathbb{C}^{NH}_{ijkl} = J^{-1}G\big[\frac{1}{2}(\delta_{ik}\bar{B}_{jl}+\delta_{jl}\bar{B}_{ik}+\delta_{il}\bar{B}_{jk}+\delta_{jk}\bar{B}_{il}) - \frac{2}{3}\delta_{ij}\bar{B}_{kl} - \frac{2}{3}\delta_{kl}\bar{B}_{ij} - \frac{2}{9}\bar{B}_{mm}\delta_{ij}\delta_{kl}\big] + K(2J-1)\delta_{ij}\delta_{kl}. \tag{12}$$

2.3.2 Transient-Viscous Tangent

Similarly, the tangent for the Linder et al. model of viscoelasticity is found via

$$\begin{aligned}
T^{neq(\alpha)}_{K,ij} &= J^{-2/3}G^{neq(\alpha)}[F_{ip}A^{(\alpha)}_{pq}F_{jq} - \frac{1}{3}(A^{(\alpha)}_{ab}F_{ca}F_{cb})\delta_{ij}] \\
\frac{dT_{K,ij}}{dF_{km}} &= -\frac{2}{3}J^{-2/3}G^{neq(\alpha)}F^{-1}_{mk}[F_{ip}A^{(\alpha)}_{pq}F_{jq} - \frac{1}{3}(A^{(\alpha)}_{ab}F_{ca}F_{cb})\delta_{ij}] + \\
&\qquad J^{-2/3}G^{neq(\alpha)}[\delta_{ik}\delta_{pm}A^{(\alpha)}_{pq}F_{jq} + F_{ip}A^{(\alpha)}\delta_{jk}\delta_{qm} - \frac{1}{3}(A^{(\alpha)}_{ab}\delta_{ck}\delta_{am}F_{cb}\delta_{ij} + A^{(\alpha)}_{ab}F_{ca}\delta_{ck}\delta_{bm}\delta_{ij})] \\
F_{lm}\frac{dT_{K,ij}}{dF_{km}} &= -\frac{2}{3}J^{-2/3}G^{neq(\alpha)}[Q_{ij}\delta_{kl} - \frac{R}{3}\delta_{ij}\delta_{kl}] + J^{-2/3}G^{neq(\alpha)}[Q_{lj}\delta_{ik} + Q_{il}\delta_{jk} - \frac{1}{3}(Q_{lk}\delta_{ij} + Q_{kl}\delta_{ij})]
\end{aligned}$$

and thus

$$\mathbb{C}^{neq(\alpha)}_{ijkl} = J^{-\frac{5}{3}}G^{neq(\alpha)}\big[-\frac{2}{3}(Q_{ij}\delta_{kl} - \frac{R}{3}\delta_{ij}\delta_{kl}) + \frac{1}{2}(Q_{lj}\delta_{ik}+Q_{il}\delta_{jk}+Q_{kj}\delta_{il}+Q_{ik}\delta_{jl}) - \frac{1}{3}(Q_{lk}+Q_{kl})\delta_{ij}\big] \tag{13}$$

where $G^{neq(\alpha)}$ is the non-equilibrium shear modulus of the α'th characteristic time, and R and Q are as defined in §2.2.

3 Update Algorithm

Denoting the beginning values of variables with a subscript n and value for the end of the time-step with subscript $n+1$, the update equations for the quantities of interest for can be written in closed form.

The intermediate metric tensor $\mathbf{A}$ evolves following Eq. 3 and time integration by an implicit backward Euler technique yields the closed-form discrete function

$$\mathbf{A}_{n+1} = \frac{1}{1+\frac{\Delta t}{\tau}}\left(\frac{\Delta t}{\tau}\bar{\mathbf{C}}^{-1}_{n+1} + \mathbf{A}_n\right) \tag{14}$$

for updating the metric tensor. Given this, the discretized viscus stress of in the network follows as

$$\mathbf{T}^{neq(\alpha)} = G^{neq(\alpha)} J^{-5/3}\left(\mathbf{Q}^{\alpha}_{n+1} - R^{\alpha}_{n+1}\mathbf{I}\right) \tag{15}$$

with $G^{neq(\alpha)}$, $\mathbf{Q}^{\alpha}$, and R^{α} are as defined above. The non-equilibrium stress is deviatoric and thus $\bar{\mathbf{T}}_{n+1} = \mathbf{T}_{n+1}$ and no bulk modulus need be specified. The update for the non-dissipative branch is

$$\mathbf{T}^{NH}_{n+1} = G^{NH} J^{-5/3}_{n+1}\left(\mathbf{B}_{n+1} - \frac{tr(\mathbf{B}_{n+1})}{3}\mathbf{I}\right) + K^{NH}(J_{n+1}-1)\mathbf{I}. \tag{16}$$

The total update for stress is

$$\mathbf{T}_{n+1} = \tau^{NH} + \sum_{\alpha=1}^{N}\tau^{neq,\alpha}. \tag{17}$$

The update for the neo-hookean tangent is

$$\begin{aligned}\mathbb{C}^{NH}_{ijkl_{n+1}} = J^{-1}_{n+1}G^{eq}\big[&\frac{1}{2}(\delta_{ik}\bar{B}_{jl_{n+1}} + \delta_{jl}\bar{B}_{ik_{n+1}} + \delta_{il}\bar{B}_{jk_{n+1}} + \delta_{jk}\bar{B}_{il_{n+1}}) \\ &-\frac{2}{3}\delta_{ij}\bar{B}_{kl_{n+1}} - \frac{2}{3}\delta_{kl}\bar{B}_{ij_{n+1}} + \frac{2}{9}\bar{B}_{mm_{n+1}}\delta_{ij}\delta_{kl}\big] + K(2J_{n+1}-1)\delta_{ij}\delta_{kl}.\end{aligned} \tag{18}$$

The algorithmic tangent update for the viscous branches, via the ABAQUS definition given above, as

$$\begin{aligned}\mathbb{C}^{\alpha}_{n+1} =& J^{-5/3}_{n+1}G^{neq(\alpha)}\big[-\frac{2}{3}(Q_{ij_{n+1}}\delta_{kl} - \frac{R_{n+1}}{3}\delta_{ij}\delta_{kl}) \\ &+\frac{1}{2}(Q_{lj_{n+1}}\delta_{ik} + Q_{il_{n+1}}\delta_{jk} + Q_{kj_{n+1}}\delta_{il} + Q_{ik_{n+1}}\delta_{jl}) - \frac{1}{3}(Q_{lk_{n+1}} + Q_{kl_{n+1}})\delta_{ij}\big]\end{aligned}$$

The total update for the tangents is

$$\mathbb{C}_{ijkl} = \mathbb{C}^{NH}_{ijkl_{n+1}} + \sum_{\alpha=1}^{N}\mathbb{C}^{neq(\alpha)}_{ijkl} \tag{19}$$

where variables have been previously defined.

With update equations in place for the stresses, the internal variables (i.e. the six unique values per non-equilibrium branch of the symmetric tensor $\mathbf{A}^{\alpha}$), and algorithmically consistent tangents the mathematical framework required to operate a UMAT is in place.

4 Model Validation

To test that the UMAT implementation functions as expected and gives rational outputs two stages of testing are employed. In initial testing the equilibrium response compared in both simple and complicated loading scenarios to the ABAQUS implementation of our equilibrium spring. In further testing, the complete response of the total network is tested against the implementation found in Wang et al. [3] for simple tension. Both cases use material parameters as specified in [3] for VHB 4910, reproduced in table 1. These parameters are obtained by Wang though fitting to the experiments of Hossain et alii [4]. For equilibrium tests $G^{neq(\alpha)} = 0$.

Table 1: *Material properties of VHB 4910 (3M Corp., St. Paul, MN) as specified for testing.*

Parameter	Value	Parameter	Value	Parameter	Value
G^{eq}	15.36 kPa	$G^{neq(1)}$	26.06 kPa	$\tau^{(1)}$	0.6074 s
K^{eq}	15360 kPa	$G^{neq(2)}$	26.53 kPa	$\tau^{(2)}$	6.56 s
		$G^{neq(3)}$	10.83 kPa	$\tau^{(3)}$	61.25 s

4.1 Equilibrium Response

4.1.1 Simple Shear

To exercise the model as completely as possible in the simple loading case for a single element, a simple shear test was conducted. In this test, a logarithmic strain of 0.5 was cyclically imposed in a pure shear mode, see the visualization in figure 2. The stress and strain in the material was monitored. This stress-strain curve is shown in figure 2. The maximum difference between the two signals is computed via

$$\%difference_{max} = \left[\frac{\max\left(\sigma_{23}^{NH}(t) - \sigma_{23}^{ABQ}(t)\right)}{\sigma_{23}^{ABQ}\left(t = t_{\max\left(\sigma_{23}^{NH}(t) - \sigma_{23}^{ABQ}(t)\right)}\right)} \right] 100\% \tag{20}$$

given applied shear in the σ_{23} loading direction. Applying this metric pointwise to the discrete-time output from ABAQUS yields a 0.0% difference in both stress and strain throughout the event history, which confirms the closely matched values seen in figure 2.

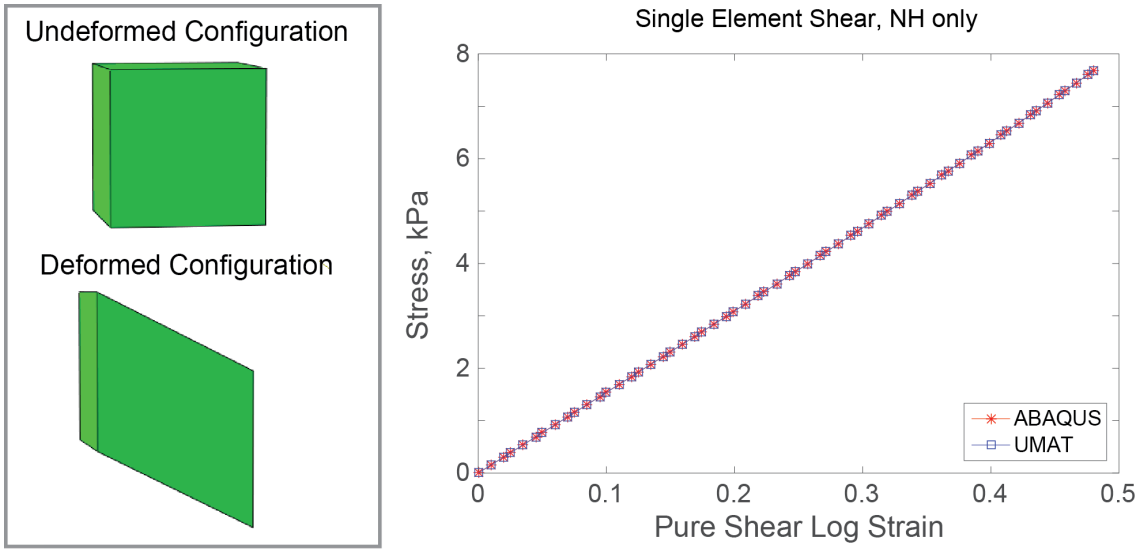

Figure 2: *The undeformed and deformed configuration of the material element and the log shear stress-strain curve for a single element. Traces show the Neo-Hookean response from the built-in ABAQUS implementation and the UMAT implementation outlined above, note the strong match.*

In the single element, the computations involving stresses in the UMAT are utilized, but the tangents do not influence the results. Thus, additional testing for more realistic geometries is required.

4.1.2 Curved Bar

A comparison between the ABAQUS and UMAT implementations for a curved bar in transverse loading was also constructed. This geometry more completely assess the models, as inhomogeneous deformations are present. In this test case, loads and displacements are tracked for a point at the extremes of the bar. A visualization of the deformation is given in figure 3 with the node of interest marked as a red dot. The load-displacement curve for both the built-in neo-hookean model and the neo-hookean model implemented here are also shown.

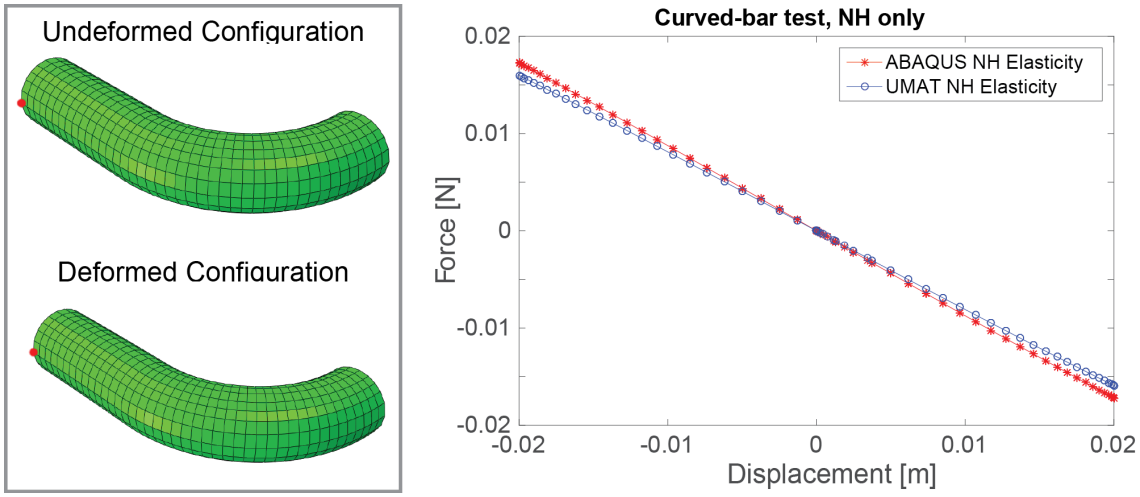

Figure 3: *The undeformed and deformed configuration of the curved bar, note the node of interest marked in red. Traces show the neo-hookean response from the built-in ABAQUS implementation and the UMAT implementation outlined above.*

There is a disparity between the neo-hookean responses shown in figure 3. Although both constitutive models follow the same basic procedure and ought to be identical, a difference of 7.47% arises in this multi-element test. The cause of the discrepancy is likely to be a result of differences in applying converges criteria between built-in and UMAT solvers in ABAQUS. To support this hypothesis, a test showed decreasing anomalous non-zero noise in the transverse stress for a single-element model in simple tension, see figure 4.

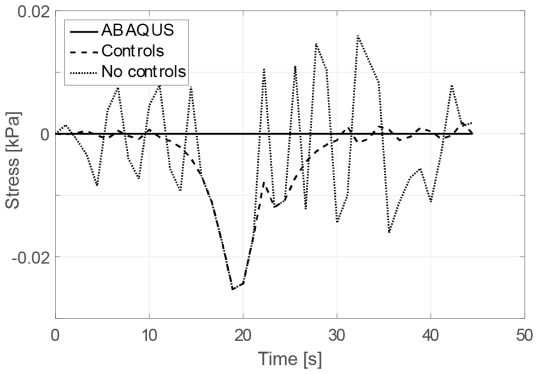

Figure 4: *Transverse stress versus time for a simple uniaxial experiment. Note the decreased noise with stricter convergence controls.*

4.1.3 Notched Plate

A final further multielement test case was conducted to assess the nature of the differences observed previously. In this case a notched bar geometry was tested in a tension-compression experiment to 20% strain, see figure 5. This geometry also yields an inhomogeneous state of stress and yields a highly nonlinear load-displacement curve. The load and displacement were measured on a fiducial node of the displacement controlled surface.

The maximum difference between the UMAT and the ABAQUS output for this case was 2.72%. The differences do not appear to be related to strain magnitude and are likely to remain relatively small across inhomogeneous loading modes, given the observed characteristics.

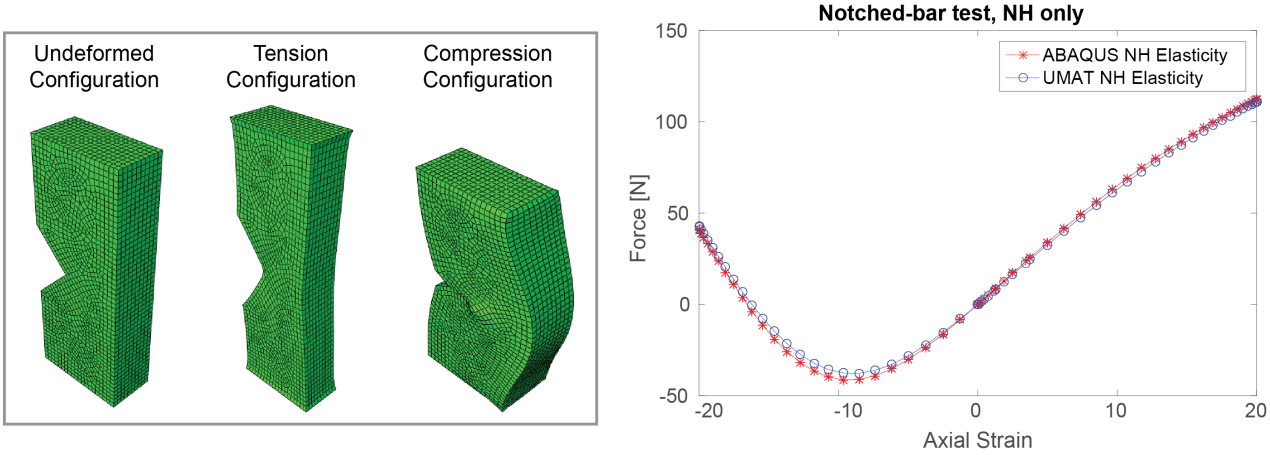

Figure 5: *The undeformed and deformed configurations of the notched bar. Traces show the Neo-Hookean response from the built-in ABAQUS implementation and the UMAT implementation.*

4.2 Complete Network Response

As a validation of the model, results for the complete network are compared against a similar model by Wang et al. [3], which was the source of the material parameters in table 1. The Wang et al. model uses three Linder et alii-type non-equilibrium branches and an Arruda-Boyce equilibrium branch, in contract to the neo-hookean equilibrium spring of the present work. To compare the fitted response data, the computations of Wang et al. were digitized by hand and are been plotted with data from the present work in figure 6. To fully compare the simple tension response three stretch amplitudes ($\lambda = 1.5, 2.0,$ & 3.0) and four stretch rates ($\dot{\lambda} = 0.9 \times 10^{-4}, 0.01, 0.03,$ &0.05) are shown.

Generally strong agreement is observed between the results of Wang et al. and the present work. Although Wang et al. have given data for up to $\lambda = 9$ for the quasistatic ($\dot{\lambda} = 0.9 \times 10^{-4}$) case, the neo-hookean model is unable to capture the polymer locking and diverges substantially from reality after $\lambda = 3$. There exists three primary sources of differences between the two datasets. First, the digitization process leads to c.$\pm$2kPa error on the data from Wang et al. Second, the underprediction of forces by the neo-hookean branch leads to notably smaller stress, particularly for the $\lambda = 2$ and $\lambda = 3$ cases. Third, as was discussed above for the neo-hookean comparison, convergence criteria or other subtle differences may arise between the user-element subroutine of Wang et al. and the UMAT implementation used in the present work.

5 Test Cases

5.1 Hysteresis

As an initial test case, hysteresis in a uniaxial test specimen was conducted. Two strain rates were tested for two stretch amplitudes, for three-cycles. The results are shown in figure 7.

In this test, a small amount a strain hardening occurs, which mostly occurs during the initial strain cycle. These changes are most noticeable in tension, even for the fully-reserved case. Higher strain rates seem to be associated with greater inter-cycle variation. This behavior is is consistent with the observations made by Linder et al. in their 2011 publication.

5.2 Hole-Plate

An inhomogeneous test case often used to test finite element implementations is the hole-in-a-plate geometry. The results of such a test for the model implement here is shown in figure **??**.

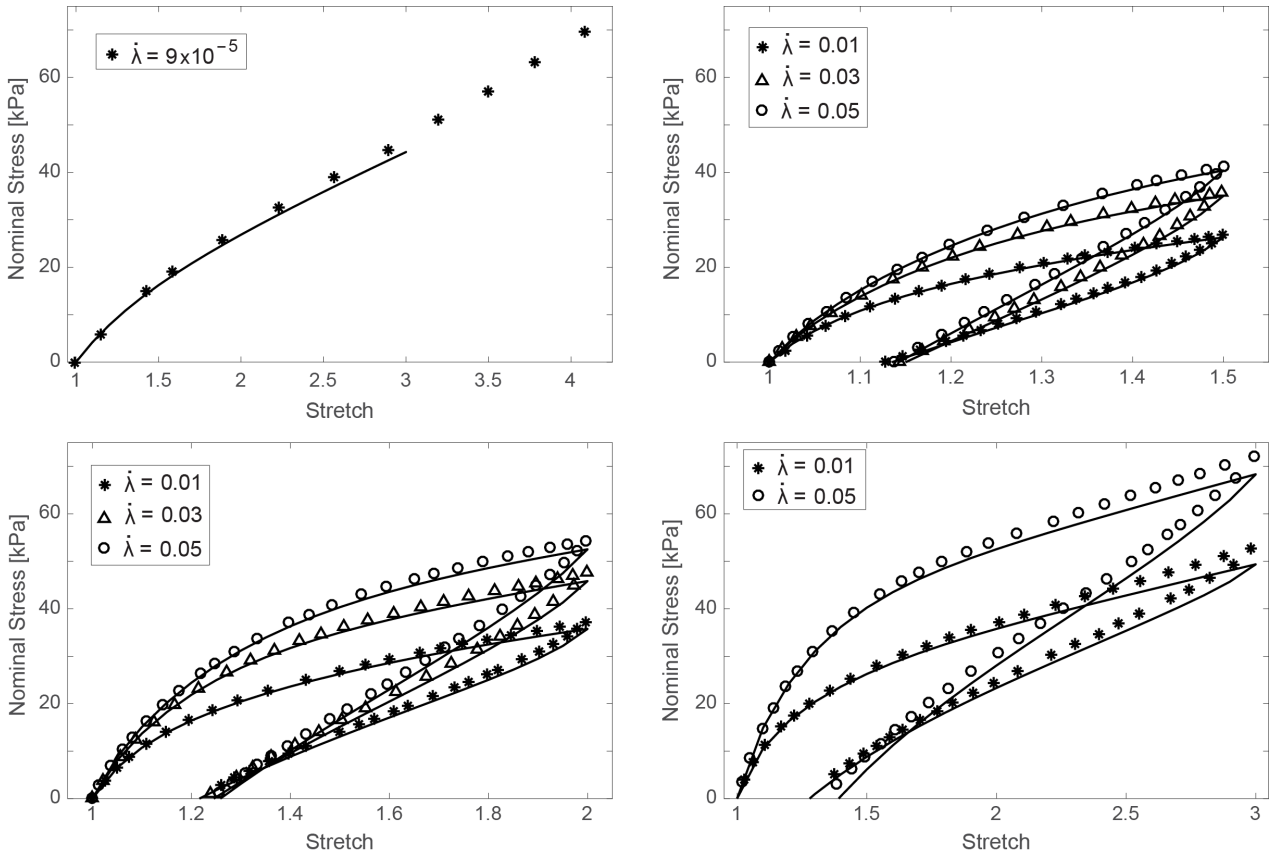

Figure 6: *Complete network response curves for several stretch amplitudes and rates. Solid lines show the results from the present work, and symbols show data from Wang et alii's computations, both use data for VHB 4910 given in table 1. The intermediate rate for large stretch was unavailable in the original experimental work of Hossain et al. and is thus not reproduced here.*

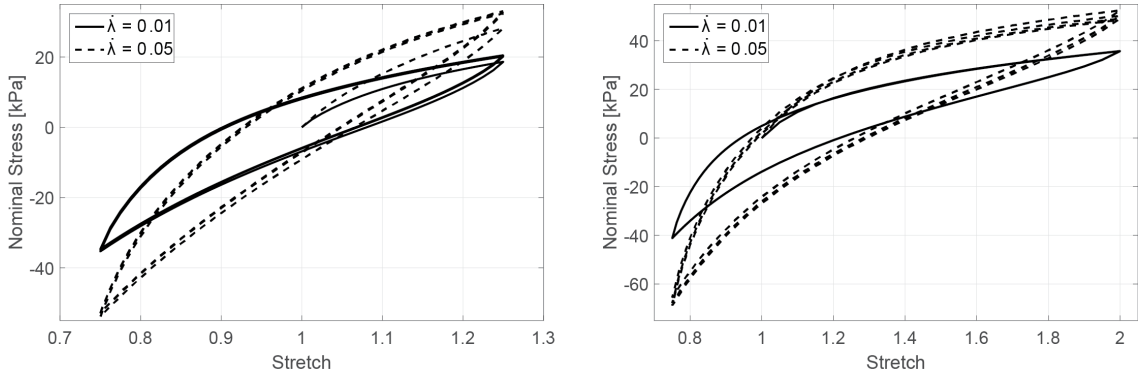

Figure 7: *Hysteresis curves for various strains amplitudes and rates. Note that a small amount of strain hardening occurs, but following the first cycle little further effect is observed. Inter-cycle variations are generally larger for higher strain rates.*

5.3 Notch-Plate

A final inhomogeneous test case of a notched plated is shown in **??**.

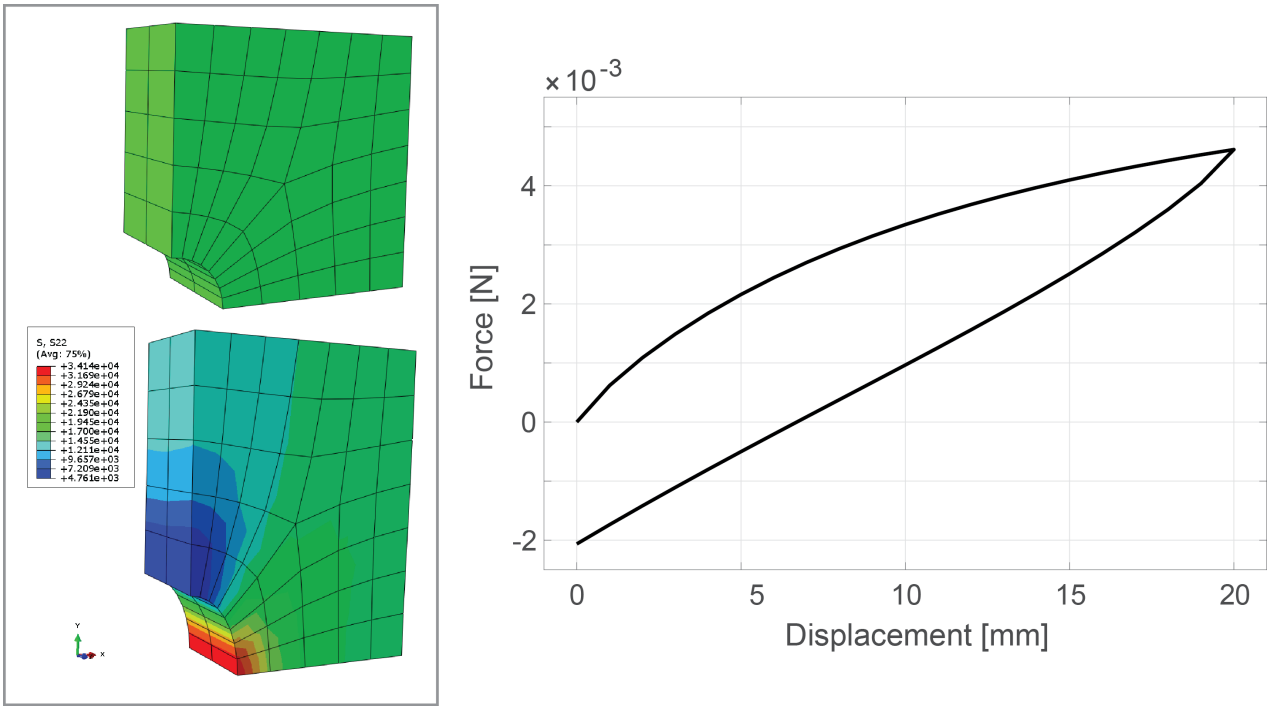

Figure 8: *Undeformed and deformed views of the hole-plate inhomogeneous loading experiment. The load-displacement for a node selected on the top face is also shown. The specimen is 0.1m x 0.1m x 0.05m in the undeformed configuration.*

6 Conclusions

References

[1] Linder, C., Tkachuk, M., and Miehe, C., 2011. "A micromechanically motivated diffusion-based transient network model and its incorporation into finite rubber viscoelasticity". *Journal of the Mechanics and Physics of Solids,* **59**(10), pp. 2134–2156.

[2] Doi, M., and Edwards, S., 1988. *The theory of polymer dynamics*, Vol. 73. Oxford University Press.

[3] Wang, S., Decker, M., Henann, D., and Chester, S., 2016. Modeling of dielectric viscoelastomers with application to electromechanical instabilities. Submitted.

[4] Hossain, M., Vu, D. K., and Steinmann, P., 2012. "Experimental study and numerical modelling of vhb 4910 polymer". *Computational Materials Science,* **59**, pp. 65–74.